



Nano-sized Titanium-zirconia Catalyst Modified by Sulphate as an Efficient Catalyst



Sh. M. El-Dafrawy

Chemistry Department, Faculty of Science, Mansoura University, Mansoura, Egypt.

A SERIES of sulphate modified titanium zirconia catalysts was set up by a sol-gel technique. All samples were calcined at several temperatures of 500, 600, and 750°C for 3h. The investigation methods of structural characteristics were used such as; thermal analysis, powder X-ray diffraction (XRD), transmission electron microscope (TEM), and Scanning electron microscope (SEM). In addition, the textural features were evaluated from low temperature adsorption of N₂ at -196 °C. The measurement of surface acidity was determined with non aqueous titration of n-butylamine in acetonitrile. Peckman condensation for production of cumarin was used in testing the catalytic activity of the constructed catalysts. The photo degradation of methylene blue dye using sulphate modified zirconia titanium catalyst was investigated.

Keywords: Sulphate modified titanium zirconia catalyst, Surface acidity, Sol-gel method, Catalytic activity, Photodegradation.

Introduction

Highly disperse (nano particulate) oxide amalgamations are of major attention for different implementations. Due to the strength of surface active sites and heterogeneous catalysts with a variable set [1] furthermore, they are a portion of inorganic-organic composites and polymer fillers [2]. In addition, integration of different oxides grants to generate active sites on the surface that are missed in single constituents. Active sites of solid acid catalysts tincture are distinct by mobile surface protons creating Brønsted acid sites and synchronize unsaturated cationic centers as Lewis acid sites [3]. Consequently, bilateral and/or triplex metal oxides are taken concerned awareness to develop heterogeneous catalysts.

Therefore, the key goal to synthesis these nano scale structures is targeted at managing their structures of surface and the morphology of particle. The mixture of titania and zirconia has appeal more interest in contemporary times. Oxides of TiO₂-ZrO₂ have been widely applied as

catalysts and catalyst supports for a widespread diversity of reactions [1]. The composites of these mixed oxides are utilized as photocatalysts because of a minimization of band gap in comparison to single components [4-6]. These mixed oxide composites have been illustrated to display an extraordinary acidity because of the lack of harmony of charges due to the Ti-O-Zr bridges formulation [5]. Sulphate modified titanium zirconia composites (STZ, SO₄²⁻/ZrO₂-TiO₂) are distinguished by higher acidic characteristics other than individual ingredients. A system of TiO₂-ZrO₂ is a potent solid acid appearing catalytic efficiency in reactions as pechman condensation reaction [7-8]. The present study aimed to adopt a sulphate modified titanium zirconia catalyst (STZ, SO₄²⁻/ZrO₂-TiO₂) system as a catalyst, and also photocatalyst. The modified catalytic systems (SO₄²⁻/ZrO₂-TiO₂) were then applied to the preparation of 7-hydroxy-4-methyl coumarine, synthetic coumarine displays potential usage in cancer therapy, mainly in dermal malignance.

Corresponding author e-mail: shomirage@yahoo.com

Received 28/4/2019; Accepted 21/5/2019

DOI:10.21608/ejchem.2019.12363.1768

© 2019 National Information and Documentation Center (NIDOC)

Experimental

Materials

All chemicals "organic & inorganic" (zirconium oxy chloride, Ethanol, Ammonium hydroxide, Ammonium sulphate, and titanium isopropoxide) used in the preparation steps of catalysts were of analytical grade. Also organic compounds used in catalytic conversion experiments were chromatographically pure.

Preparation of Catalysts

Preparation of Zirconia Titanium Catalyst

To prepare titanium zirconia hydroxide, zirconium oxy chloride and titanium isopropoxide (1:1) were dissolved in absolute ethanol solution, and 33% solution of NH_4OH act as precipitating agent. Ammonia solution was heated on water bath and its vapour pass through zirconium and titanium salts with continuous stirring until the $\text{pH} = 9.5$. The precipitated gel was continuously stirred for 1 h after the precipitation has been completed, then dried for a suitable time, then calcined at 500°C for 3 h.

Preparation of Sulphate Modified Zirconia Titanium (STZ) Catalyst

Different percentages of $(\text{NH}_4)_2\text{SO}_4$ solution was prepared and added to $\text{ZrO}_2/\text{TiO}_2$ as sulphating agent with different percentage to obtain (2, 8, 15, 25 and 40) wt % SO_4^{2-} samples.

Drying and Calcination of the STZ Catalyst

All of the prepared catalyst samples were dried at 120°C for about a suitable time. The solid was pulverized and screened to 0.4-1.25 mm particle size. The prepared catalysts were calcined at 500, 600, and 750°C for 3h.

Techniques

X-Ray diffraction analysis

X – Ray study [9] was performed for the investigated catalysts via a Philips apparatus PW 105 diffractometer by Ni-filtered Cu K α radiation ($\lambda = 1.540 \text{ \AA}$) at operating voltage 40 kV, 30 mA. All samples were scanned with speed 2° min^{-1} from 2θ of 5 to 80° .

Surface acidity measurements

Non aqueous potentiometric titration

The n-butyl amine titration technique was used for determination of the total acidity of all catalysts by an Orion 420 digital A model with a double junction electrode [10-11].

Pyridine adsorption using FTIR spectra

The samples FTIR spectra were done at room temperature by degassed 0.05 g of every

sample at 250°C for around 2 hrs to lower the adsorbed molecular water amount. Following, the evacuation the samples were sustained in contact with pyridine vapor at room temperature for suitable time [12].

Thermal analysis

Differential thermal analysis (DTA) and Thermogravimetric analysis (TGA) was carried out with the aid of Thermo analyzer (D-50) shimadzu, Japan [13].

Nitrogen adsorption measurements

The adsorption-desorption isotherms of nitrogen gas were determined at its boiling point (-196°C) by means of a conventional volumetric apparatus. The apparatus consists of two parts, the vacuum system and the adsorption system. The vacuum system consists of an oil rotary high vacuum pump, followed by a mercury diffusion pump. By this combination it is possible to reach pressures as low as 10^{-4} mm Hg. This is determined by a McLeod system connected to the apparatus [14].

Morphology determined by Transmission electron microscope (TEM)

TEM was applied by a JEOL 2010 apparatus with resolving power 0.2 nm and accelerating tension being 200 keV. Reflectance UV-vis spectra were collected and converted to absorbance by Perkin-Elmer Lambda 9 scanning spectrometer apparatus with an integrating sphere over the spectral range 200-2500 nm (6.2-0.5 eV). In this study the band gap energies quoted are based on Shapiro's technique [15].

Catalytic activity measurements studied by Pechmann Coumarine synthesis

The catalytic activities of the investigated samples were studied by Pechmann condensation reaction. In a regular experimentation, a mixture of resorcinol (1.1 g, 10 mmol) and ethyl acetoacetate (2.5 ml, 20 mmol) was putted in a round flask of 50 ml. This reaction mixture was transferred into oil bath and refluxed at 120°C for 2h [16-18]. The product yield was accounted according to the following equation (1):

$$\text{yield (wt \%)} = \frac{\text{obtained weight of product}}{\text{theoretical weight of product}} \times 100 \quad (1)$$

Evaluation of photocatalytic activity

The evaluation of synthesized photocatalysts was done by the methylene blue dye (MB)

degradation under UV/Vis irradiation. A 400 W Hg lamp was standing at 20 cm from the reaction system and the temperature of reaction was retained lower than 35 °C. The photocatalyst (0.1 gm) was suspended into 50 ml of MB aqueous solution ($C_0=10 \text{ mgL}^{-1}$). Then the reaction mixture was magnetically stirred in dark for 1 h to reach the adsorption-desorption equilibrium before light turning [19]. The degradation rate was estimated from the following equation (2):

$$D\% = \frac{(C_0 - C_t)}{C_0} \times 100 \quad (2)$$

Where D is the degradation rate (%), C_0 and C_t are the concentrations of the MB solution at $t = 0$ and $t = t$, respectively.

Results and Discussion

Differential Thermal Analysis (DTA) of the STZ Samples

As shown in Fig. 1, the first step weight loss, accompanied by an endothermic peak around 30 to 180°C, can be assigned to the removal of physisorbed water and ethanol [20]. The DTA curves of the samples also show a peak around 200-300°C. These effects could be attributed to the alkoxide residues elimination which is predominant in all STZ samples, this may be due to the eliminated alkoxy-function (as alcohol) is probably evaporated throughout the step of oven drying. The DTA curves of the samples also show peak around 280-450°C. These effects are due to the evolution of ammonia on the surface as well as into the lattice [21] and the called glow-exothermic effect, attributed to the abrupt expulsion of ammonia, forms uneven fracture surface, producing practically round polyhedral partially wrapped by free deposits [22].

Differential thermal analysis (DTA) data show a single exothermic peak at 540 °C for pure $\text{ZrO}_x(\text{OH})_{4-2x}$. While after addition of SO_4^{2-} the exothermic peak shifted to 700°C [23], corresponding to crystallization into solid $\text{ZrO}_2\text{-ZrO}_x(\text{OH})_{4-2x}$ samples. The DTA minimum peaks which appear at higher temperature might be because of the evolution of SOx decomposed from sulphate ions joined to the surface of titania and zirconia, these minimum peaks are accompanied by weight loss around 500-800°C.

As described previously, the addition of titania or sulphate to zirconia system improves the thermal

stability, the alterations in crystallization kinetics have been reflected by the shift of the exothermal DTA peaks to the greater values. Also addition of titanium in STZ series shifts the exothermic peak which corresponds to the crystallization to higher temperature.

X-ray Diffraction Analysis

Effect of Sulphate content on X-ray Diffraction Analysis of STZ Samples

Figure 2 shows that, all the samples were amorphous even by increasing the SO_4^{2-} content and this was confirmed by the thermo gravimetric analysis and differential thermal analysis, which didn't give a phase corresponding to crystallization peak until the temperature rises to 600°C (Fig. 2). This was confirmed also by DTA showing that the crystallization peak appears at 700°C. The crystalline phase of STZ appears at 750 °C as illustrated in Fig. 3 [24].

Effect of Calcinations Temperature on X-ray Diffraction Analysis of STZ Samples

Figure 3 shows that at calcination temperatures of 500°C and 600°C the samples were amorphous. By rising the calcination temperature to 750°C [25], the amorphous phase changes to mainly tetragonal phase [26-27]. This result affirms that SO_4^{2-} group decomposition can catalyze the transformation of amorphous phase to tetragonal one at the higher temperature.

Evaluation of textural parameters via the adsorption of nitrogen by STZ samples

Effect of SO_4^{2-} content on the specific surface area of STZ samples

The sulphate addition to zirconia was noted to raise the thermal resistance of the high surface area amorphous or crystalline phase versus sintering. Also, it was shown that amorphous $\text{ZrO}_2\text{-TiO}_2$ mixed oxides become crystalline at the greater temperature than pure ZrO_2 [28].

For STZ samples, Fig. 4 shows the effect of SO_4^{2-} content on the values of the specific surface area. The incorporation of SO_4^{2-} into STZ samples was correlated with an increasing continuously of S_{BET} up to 15 % SO_4^{2-} loading. Further increase of SO_4^{2-} content beyond 15% leads to a decrease of SBET. This may be due to the simultaneous filling of TZ pores after addition of 15% SO_4^{2-} , where the surface area is decreased due to the SO_4^{2-} groups blocked the pores of TZ [29].

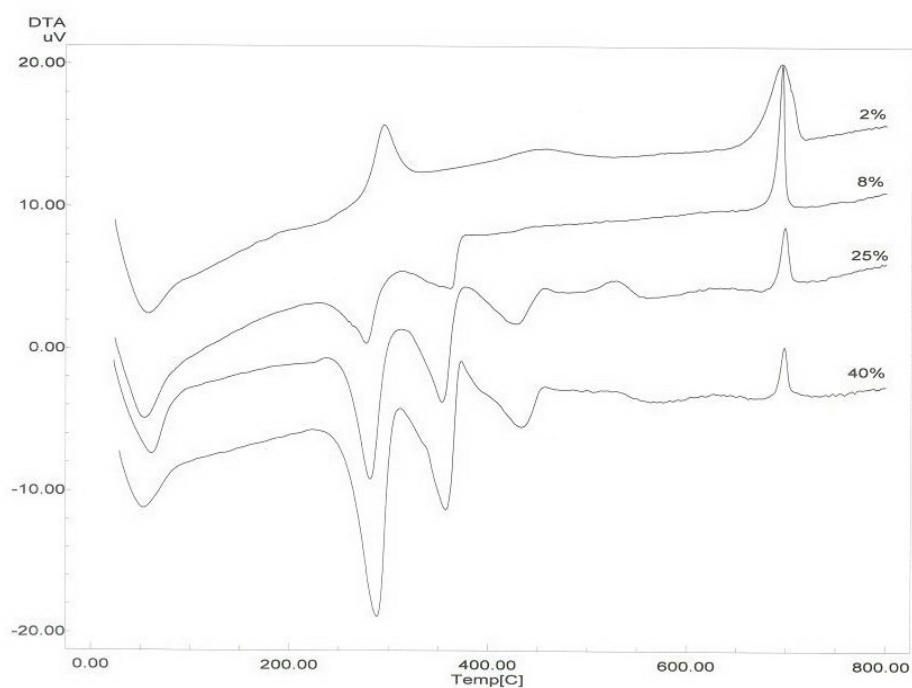


Fig. 1. Differential Thermal analysis (DTA) of the STZ with different SO_4^{2-} %

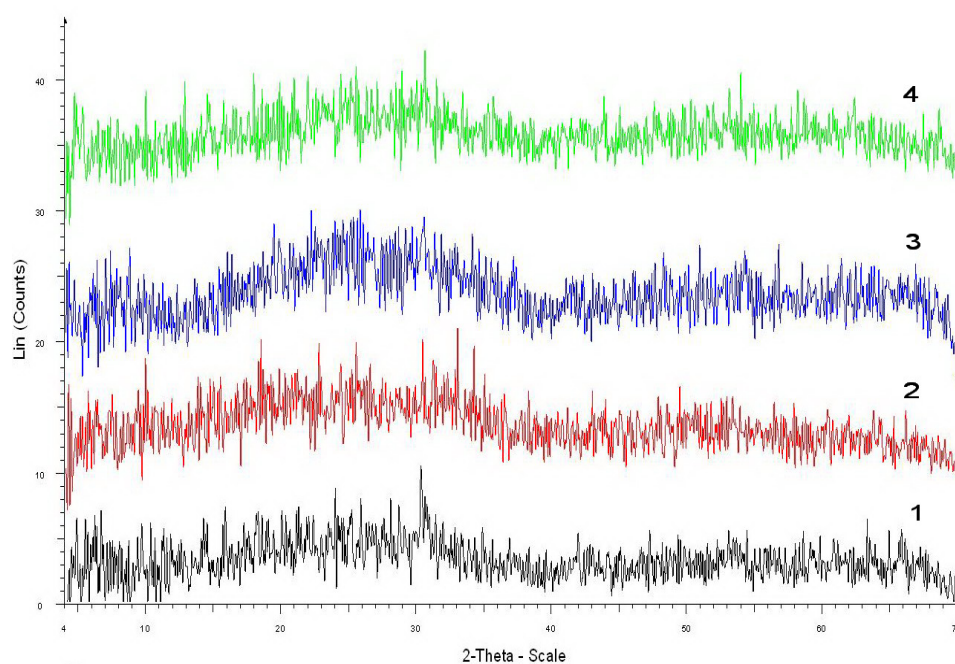


Fig. 2. X-Ray diffraction patterns of the different STZ samples calcined at 600, 1) 8 % STZ, 2) 15 % STZ, 3) 25% STZ, and 4) 40% STZ.

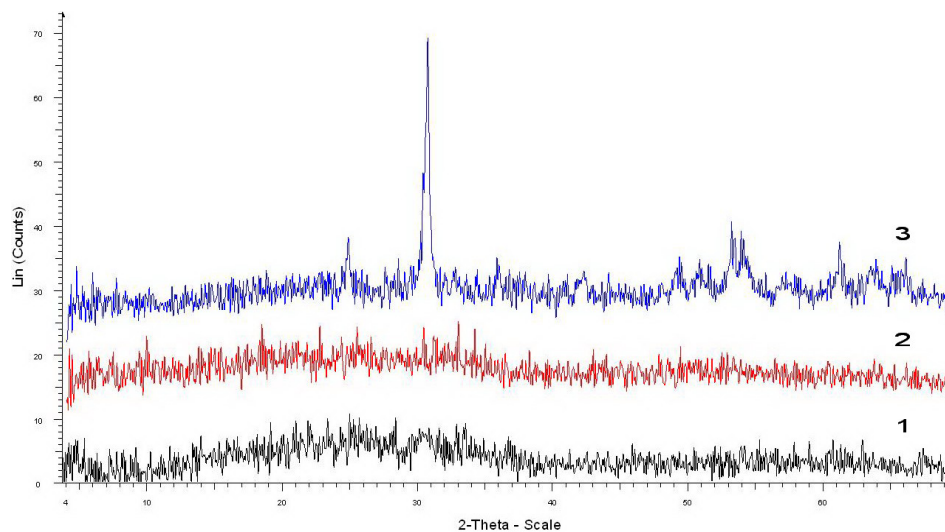


Fig. 3. X-Ray diffraction patterns of 15 % STZ samples calcined at, 1) 500°C, 2) 600 °C, and 3) 750 °C.

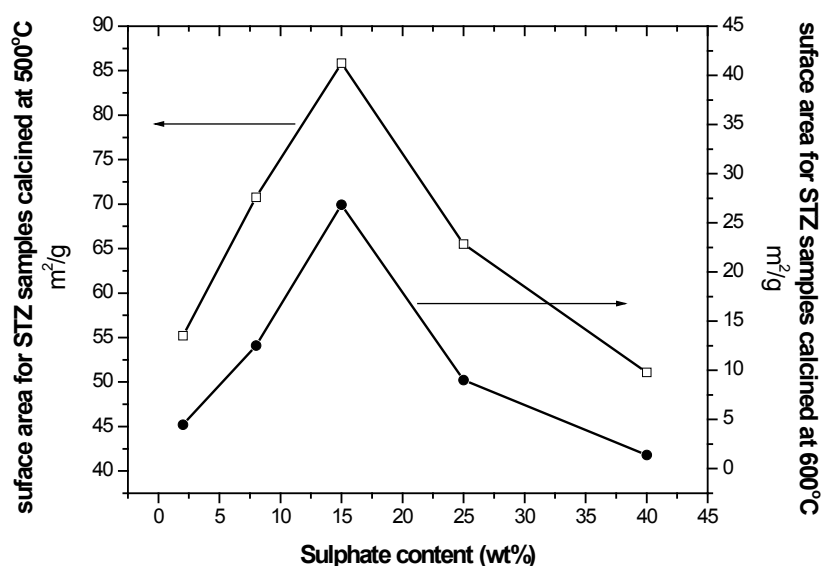


Fig. 4. Effect of SO_4^{2-} content on the specific surface area of STZ samples calcined at 500 and 600 °C.

Effect of calcinations temperature on the specific surface area of STZ samples

Effect of calcination temperatures on the porous properties of STZ samples at 500, 600 and 750 °C was shown in Table 1. Throughout the calcination, the amorphous STZ crystallizes to the ultimate kinetically convenient polymorph; the tetragonal one as it shown in X-Ray [30]. This leads to the growing of the crystallites with an ensuing collapse of the gel structure and a lowering of the surface area to diminish the surface free energy.

On another hand, the alkoxy groups carbonized by rising the temperature are estimated to be burnt off by the oxygen stream, generating new porosity. Consequently, the interplay between the crystal growth-structure reorganization and the residue burning-pore opening process is at the origin of this feature

Correlation between α_s and T plots with S_{BET}

Table 1 summarizes the correlation between α_s - and t -plots with S_{BET} on STZ samples. As

it can be seen from the table, the orders of the arrangement of the evaluated values of S_{BET} are in good agreement with that of S_{α_s} and S_t as shown in Table 1. This exhibits the validity of the different techniques, i.e. BET, α_s and t-techniques for the evaluation of surface area. The difference between the values of S_{BET} and S_{α_s} may be due to the values of S_a of the reference solid material.

Morphology characterization by Transmission Electron Microscope (TEM)

Effect of SO_4^{2-} content on the Morphology characterization of STZ samples by Transmission Electron Microscope (TEM)

The effect of increasing sulphate content on the crystallite size of STZ samples was characterized as shown in Fig. 6. TEM images indicate that the particle size of STZ samples were in the nano scale. By increasing the SO_4^{2-} content from 8 to 40 wt.%, it was found that the sulphate increase the ability of the particle to be more arranged to form nanotubes with diameter in range between 10-14 nm, which perform a significant action in enhancement the catalytic activity for STZ samples. Where, the formation of the nanotubes in the 40% STZ sample could exhibit high catalytic activity [31-33].

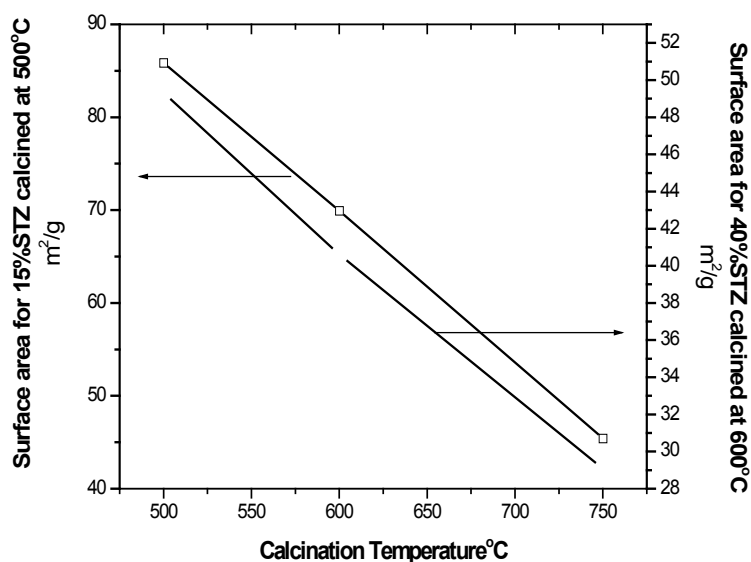


Fig. 5. Effect of calcination temperatures on the specific surface area on 15% STZ and 40%STZ samples

TABLE 1. Surface Characterization of STZ Samples.

Samples	S_{BET} m ² /g	S_{α_s} m ² /g	S_t m ² /g
2 STZ 500 °C	55.2	55.0	55.1
15 STZ 500 °C	85.85	85.80	85.83
40 STZ 500 °C	51.08	51.00	50.99
15 STZ 600 °C	69.93	69.90	69.91
15 STZ 750 °C	45.2	45.1	45.3

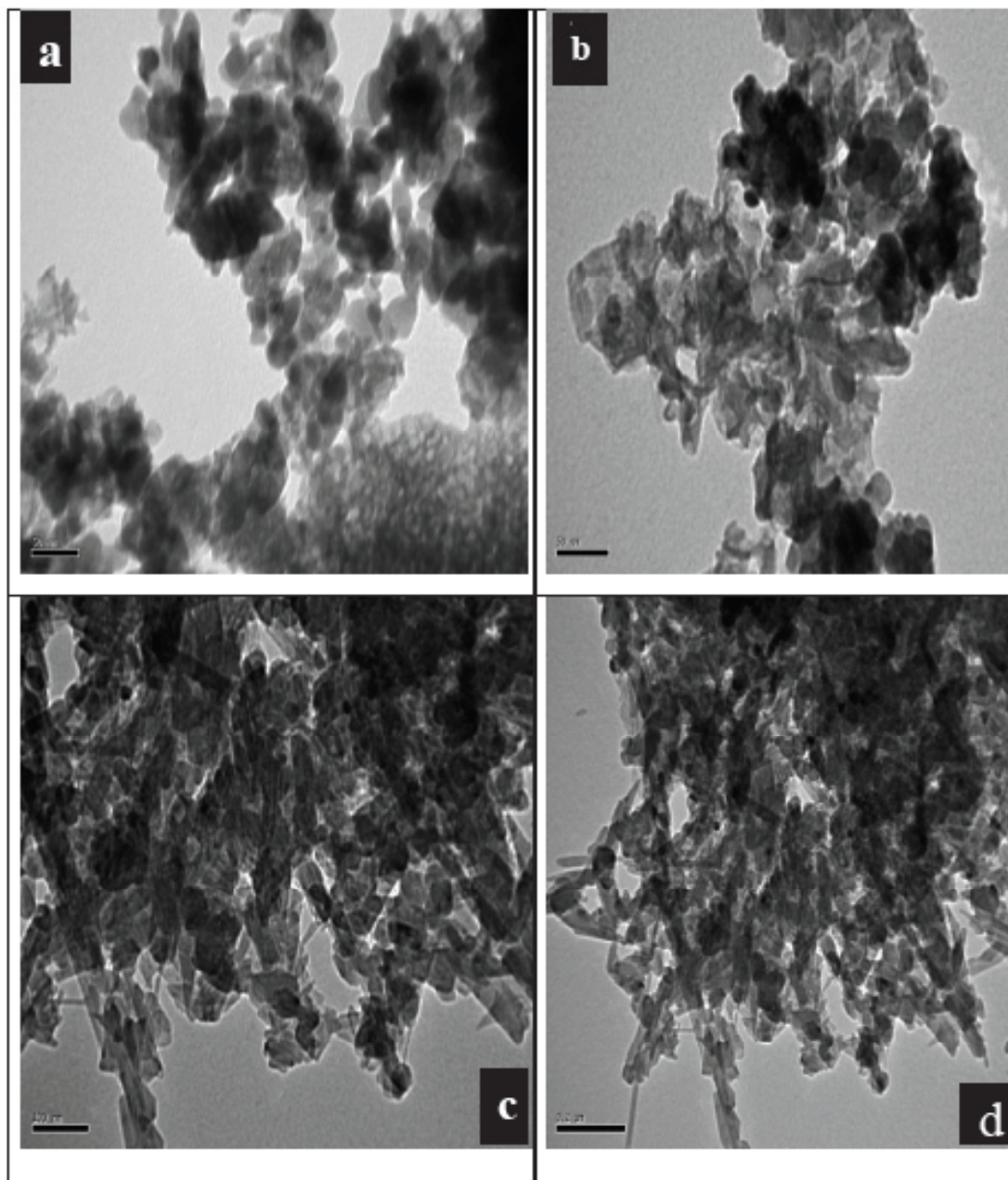


Fig. 6. TEM images of STZ Samples calcined at 600 °C, a) 8 % STZ, b) 25 % STZ, c) 40 % STZ d) 40 % STZ.

Measurements of Surface Acidity

Potentiometric titration

Effect of SO_4^{2-} Content on Surface Acidity

Measurements of STZ Samples

It was shown from Table 2 that, the addition of SO_4^{2-} can enhance the acidity of TZ samples, creating on the surface strong acidic sites. By means of a criterion to understand the acquired data, it was recommended that, the initial electrode potential (Ei) [34] signify the maximum acid

strength of the sites and the value of mleq amine/g solid where the plateau is attained indicating the total number of acid sites. The total number of acid sites/g catalyst and the values of Ei are recorded in Table 2 for samples calcined at 500 and 600°C respectively. The combination of SO_4^{2-} in ZrO_2 affects the acidity of the catalysts. Adding of sulphate to TZ was attended by a regular raise of mutually number of Brønsted acid sites and strength of acid sites to accomplish supreme at

40% STZ at which $E_i = 539.7\text{mv}$. Additionally, the samples calcined at 500°C revealed the more acidity and comparatively more acidic strength.

Effect of Calcination Temperatures on Surface Acidity Measurements of STZ Samples:

Table 2 shows that at 500°C the samples exhibit higher acidity. Additional rise in the temperature of calcination to 600 and 750°C was attended with a decline in the strength of acid. This could be due to the decomposition of the sulphate groups bonded to the surface at calcination temperature more than 500°C [35]. This gives an indication that, after decomposition of sulphate groups, the strength of the acid sites decreases.

These results exhibits that the 40 % sulphated catalysts calcined at 500°C shows a high number of acid sites and surface acidity strength. This indicates that, the dispersal and number of sulphate groups on the surface of TZ samples

are ultimate and being in authority for the greater acidity at 500°C .

Pyridine Adsorption by FTIR

Effect of SO_4^{2-} Content on Pyridine Adsorption by FTIR for STZ Samples:

For additional knowledge round the active species of surface sulphur modified on TZ, FT-IR spectroscopic examinations were implemented on 8, 15, 25 and 40 % sulphated samples calcined at 600°C , (Fig. 7). These results indicate that a Brønsted acid site (1541 cm^{-1}) enhances with an increase of the inserted amount of sulphate content. At low SO_4^{2-} content the Brønsted acid sites located around (1541 cm^{-1}), further increase in sulphate content shift the band to higher wave length more than (1620 cm^{-1}). This indicates that the strength of Brønsted acid sites increase progressively with increase in sulphate content. Also the acid sites strength (E_i) depends mainly on the sulphate content as it shown in Table 2.

TABLE 2. The effect of different sulphate content on the surface acidity of STZ samples calcined at 500 and 600°C .

Samples	m.v at zero addition	ml added	No ^o of Acid sites $\times 10^{19}$	Coumarin %
2 STZ- 500°C	235.00	0.52	1.56	40.12
15 STZ- 500°C	430.20	2.69	8.09	72.82
40 STZ- 500°C	539.70	0.92	2.75	99.32
2STZ- 600°C	12.20	0.08	2.41	16.10
15 STZ- 600°C	347.80	0.22	6.62	34.90
40 STZ- 600°C	424.90	0.18	5.36	50.24

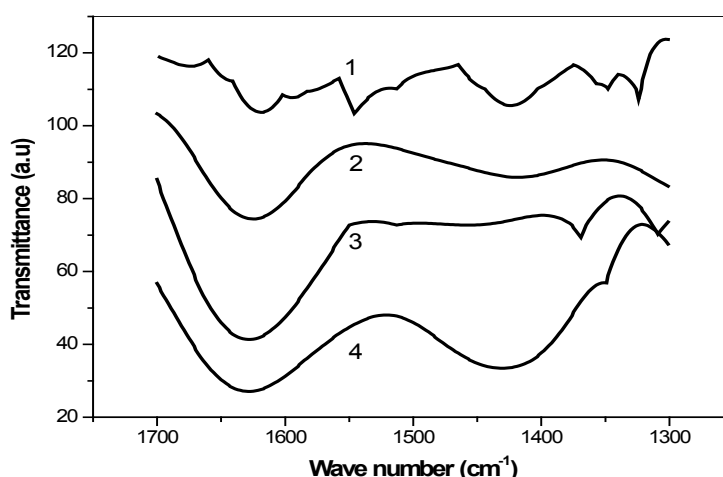


Fig. 7. FT-IR spectra of pyridine adsorbed of the different STZ samples calcined at 600°C ; (1) 8% STZ, (2) 15 % STZ, (3) 25% STZ, and (4) 40% STZ.

These results can be described in expressions of surface heterogeneity of the TZ samples; resulting to sulphate groups of little dissimilar spectroscopic signatures, as of isolated ones to polynuclear ones, as it was seen from the DTA profiles of STZ samples per altered sulphate content. Where, the figure displays dissimilar activities for the decomposition of sulphate species on the zirconia surface. From the comparison of DTA of the solids content 8, 15, 25 and 40 % sulphates, it is obvious the appearance of several peaks, when the concentration of sulphate rises. Where this is probably related to the decomposition of sulphate groups on TZ surface with altered structures.

Effect of Calcination Temperatures on Pyridine Adsorption by FTIR of STZ Samples

The result of calcinations temperature on the number of Pyridine Adsorption of 15% STZ samples were shown in Fig. 8. The relative intensity of the band characteristic to pyridine adsorbed on Brønsted acid sites decrease gradually with the temperature rise of the calcination. At lower

calcinations temperature, the band corresponding to Brønsted acid sites were shifted to higher wave length (1640 cm^{-1}). By increasing the calcination temperature the band related to Brønsted acid sites were switched to lower wave length (1600 cm^{-1}), which give an indication that the number and the strength of Brønsted acid sites decrease. Table 2 shows that, by increase the calcinations temperature the number of acid sites decreases, also the strength of acid sites decrease. This is might be because of the total number of acid sites and its strength depends mainly on the number of Brønsted acid sites.

Catalytic Activity

Effect of SO_4^{2-} content on Catalytic Activity % of STZ Samples

Figure 9 shows the correlation between the number of acid sites and the coumarine %. SO_4^{2-} increases the acidity of STZ samples, creating strong acidic sites on the surface [36]. Also the increase in the number of Brønsted acid sites is responsible for increasing the catalytic activity to 40% SO_4^{2-} as depicted in Fig 10.

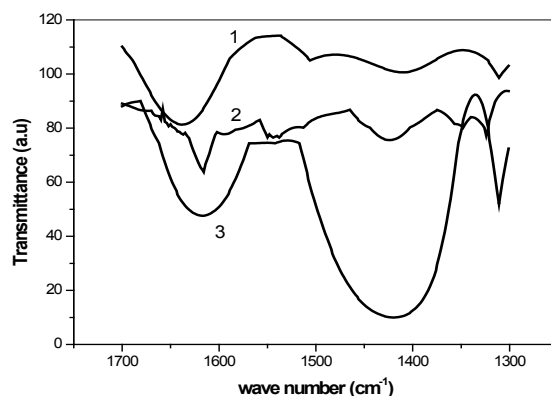


Fig. 8. FT-IR spectra of pyridine adsorbed of 15% STZ samples, (1) 500°C, (2) 600°C, and (3) 750°C

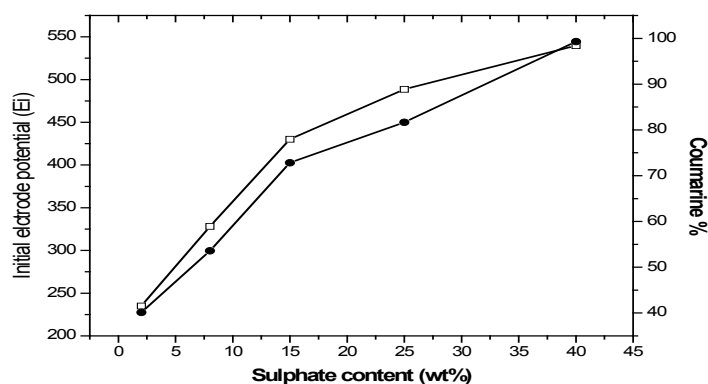


Fig. 9. Effect of sulphate content on catalytic activity % and Initial electrode potential (Ei) for STZ samples calcined at 500°C.

The activity for STZ can be explained due to the increasing in the strength of acid sites and the number of bronsted acid sites. Also the catalytic activity for STZ samples is affected by the X-Ray and is in a good agreement with it due to the phase transformation from amorphous to crystalline zirconia phase, which is accountable for the alteration in the strength distribution of the acid sites.

Effect of calcination temperatures on Catalytic Activity % of STZ Samples:

Figure 11 displays the effect of calcinations temperature on coumarine synthesis by 40 % STZ

samples. The figure showed that the coumarine yield (%) decreases by increasing the calcinations temperature, at lower calcination temperatures to 500°C, the yield of coumarine % reached to 100%. By increasing the calcination temperature to 600°C, the yield of coumarine % reached to 50%. Further increase in the calcination temperature to 750°C, the yield of coumarine % reached to 20%. This is due to by raising the calcination temperatures the number of Brønsted acid sites decreased. This improved that the coumarine synthesis (Pechmann condensation) depends mainly on the number of Brønsted acid sites

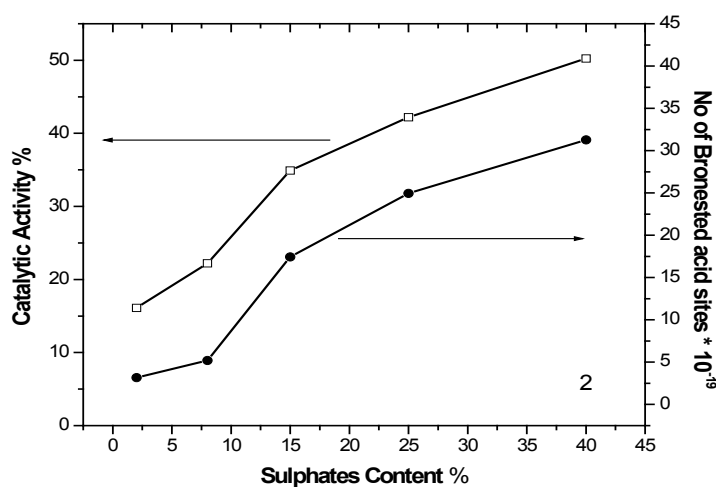


Fig. 10. Effect of sulphate content on catalytic activity % and number of bronsted acid sites for STZ samples calcined at 600°C.

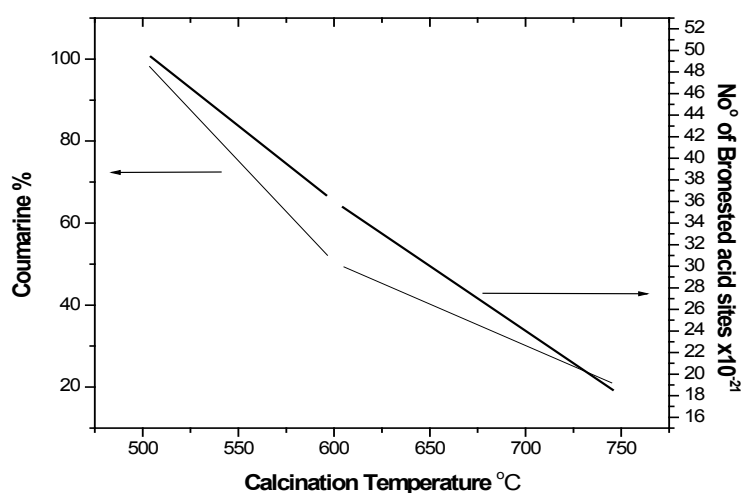


Fig. 11. Effect of Calcination Temperature on coumarine % and number of Brønsted acid sites for 40% STZ samples.

Photocatalytic Activity

Effect of Different SO_4^{2-} Concentration on MB Degradation

Figure 12 displays the photocatalytic performance of TZ with dissimilar concentrations of SO_4^{2-} calcined at 500 °C. As observed from the figure, TZ reveals a lower photocatalytic activity than STZ. This might be owing to a quickly overlap of electrons and holes, which lead to low photocatalytic activity of TZ [37].

It was observed that 15% STZ, shows the optimum photocatalytic activity. This is ascribed to the effect of SO_4^{2-} creating a new energy level into TZ [38] moreover SO_4^{2-} effect in reducing recombination rate. By raising SO_4^{2-} concentration than 15%, the activity reduced. This is due to a great concentration of SO_4^{2-} which acts as recombination centers [39, 40].

Effect of Calcination Temperatures on MB Degradation

It was observed that variation of calcination temperature result in a diversity in the photocatalytic performance. Figure 13 illustrates the photocatalytic activity of 15% STZ calcined at 500, 600, and 750°C. It is shown from Fig. 13 that 15% STZ calcined at 500°C has the optimum activity assuming by the results of TEM, SEM analysis and acidity measurements.

15% STZ calcined at 500°C reveals an apparent decrease in the photocatalytic activity, This ascribed to a large number of agglomerations which can prevent electrons transitions [41], a little number of acid sites (Table 2), then reducing adsorption of reactants. Beside the large band gap (3.4 eV) which might be more than the energy of the absorbed photon, then the photocatalytic reaction can be difficulty initiated and consequently reducing the photocatalytic activity.

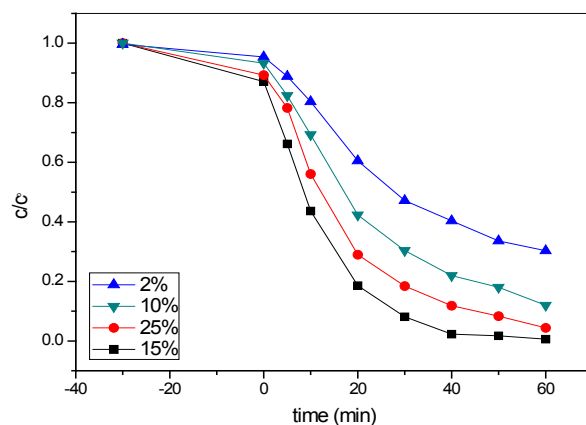


Fig. 12. Photocatalytic activity of TZ with different SO_4^{2-} concentrations calcined at 500 °C.

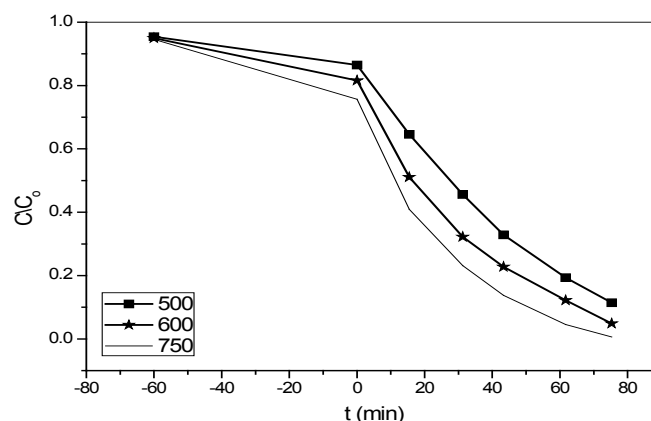


Fig. 13. Effect of calcination temperature on photocatalytic activity of 15% STZ.

Effect of pH

pH plays an obvious function in effectiveness of MB degradation as exhibited in Fig. 14. MB dye is taken into account as a cationic dye and hence its adsorption is preferred in alkaline medium [42]. Consequently, pH=10 was considered the optimum pH to conserve the stability of the MB dye.

Effect of initial MB concentration

Initial concentrations of MB (20 ppm, 50 ppm, 75 ppm and 100 ppm) were used for the investigation of dye concentration, 0.05gm of catalyst and 50 ml of dye solution at pH=10 as shown in Fig. 15. Also it can be detected that the

photodegradation efficiency reduced by rising the concentration of dye. It is well known that photodegradation efficiency basically depends on the amount of hydroxyl radicals formed on the surface of the catalyst. By means of the raising dye concentration, raising the quantity of dye adsorbed on the surface of catalyst, therefore the reduction of generation of hydroxyl radicals occurs. Additionally, rising of the concentration of MB, the less photons reach the surface of catalyst. Consequently, the production of hydroxyl radicals that can attack the pollutants will reduce and the efficiency of photocatalytic decreases [43-44].

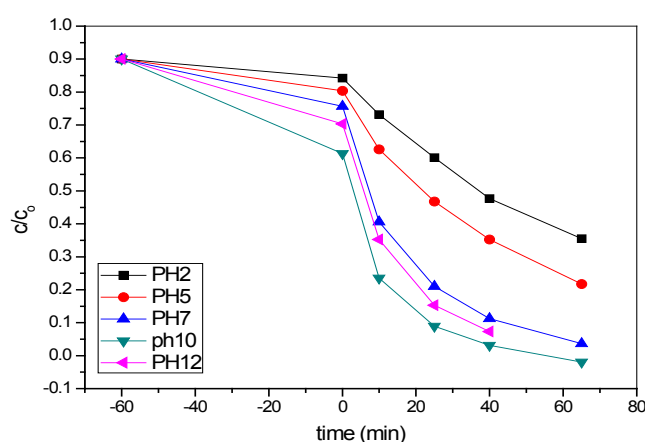


Fig. 14. Photodegradation efficiency of MB at different pH values.

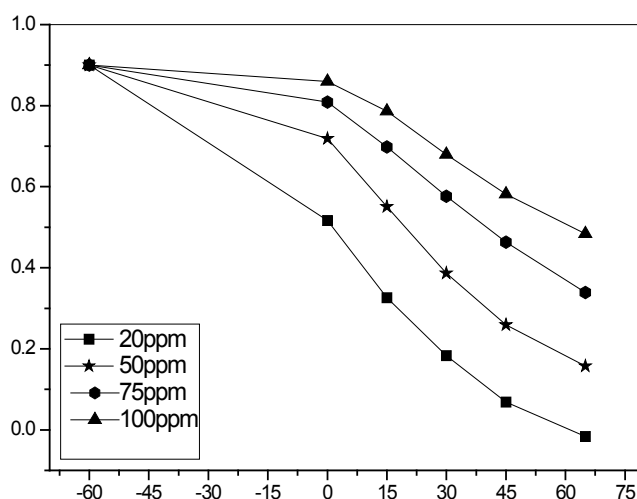


Fig. 15. Effect of initial concentrations of MB dye on the photodegradation efficiency under UV-Vis light.

Conflicts of interest

The authors declare no conflicts of interest.

Conclusions

In the existing study, sulphated titanium zirconia (STZ) samples were prepared by the precipitation method followed by calcination at different temperatures. Structural characterization and the phase changes were determined using DTA, XRD, and TEM techniques. By adding SO_4^{2-} the exothermic peak shifted from 540 to 700°C, corresponding to crystallization into solid $\text{ZrO}_2\text{-ZrO}_x(\text{OH})_{4-2x}$ samples. By increasing the SO_4^{2-} content, all the samples were amorphous, which didn't give a corresponding phase to crystallization peak until the temperature rises to 750°C. By increasing the SO_4^{2-} content from 8 to 40%, it was found that the SO_4^{2-} increase the ability of the particle to be more arranged to form nano tubes with diameter in range between 10-14 nm.

The surface area increase up to 15% SO_4^{2-} loading. The further increase in SO_4^{2-} content beyond 15% led to a decrease in S_{BET} . The surface area is decreased due to rising the temperature of calcination. SO_4^{2-} can increase the acidity of TZ samples, generating strong acidic sites on the surface, and also the increasing in the number of Brønsted acid sites were responsible for the increasing the catalytic activity upto 40% SO_4^{2-} and then decrease. The coumarine % reduction by rising the temperature of calcination to 500°C, the yield of coumarine % reached to 100%. Photocatalytic experiments showed that by increasing sulphate loading the degradation increases up to 15% SO_4^{2-} and then decreases. The photocatalytic degradation decreases by increasing the calcination temperature.

References

- Manríquez M. E., López T., Gómez R., J. Navarrete Preparation of $\text{TiO}_2\text{-ZrO}_2$ mixed oxides with controlled acid-basic properties. *J. Mol Catal A-Chem.*, **220**, 229-237 (2004).
- Hanemann T., Szabó D.V, Polymer-Nanoparticle Composites: From Synthesis to Modern Applications. *J Materials* **3**, 3468-3517 (2010).
- Corma A., Inorganic Solid Acids and Their Use in Acid-Catalyzed Hydrocarbon Reactions. *J. Chem. Rev.*, **95**(3), 559-614 (1995).
- Kim J. Y., Kim C. S., Chang H. K., Kim T.O., Effects of ZrO_2 addition on phase stability and photocatalytic activity of $\text{ZrO}_2/\text{TiO}_2$ nanoparticles. *J. Adv Powder. Technol.*, **21**, 141-144 (2010).
- Wu B., Yuan R., Fu X., Structural characterization and photocatalytic activity of hollow binary $\text{ZrO}_2/\text{TiO}_2$ oxide fibers. *J Solid State Chem.*, **182** (3), 560-565 (2009).
- Zhang M., Yu X., Lu D., Yang J., Facile synthesis and enhanced visible light photocatalytic activity of N and Zr co-doped TiO_2 nanostructures from nanotubular titanic acid precursors. *J. Nanoscale Res. Lett.* **8**, 543-551 (2013).
- Yamaguchi T., Recent progress in solid superacid, *J. Appl. Catal.*, **61**, 1-25 (1990).
- Sulym I., Goncharuk O., Sternik D., Skwarek E., Derylo – Marczevska A., Janusz W., Gun'ko V. M., Silica-Supported Titania-Zirconia Nanocomposites: Structural and Morphological Characteristics in Different Media, *J. Nanoscale Resear. Lett.*, **11**, 111-120 (2016).
- Ahmed A. I., El-Hakam S. A., Samra S. E., EL-Khouly A. A., Khder A. S., Structural characterization of sulfated zirconia and their catalytic activity in dehydration of ethanol. *J. Coll. and Surf. A: Physicochem. Eng. Aspects*, **317**, 62-70 (2008).
- Suryanarayana I., Reddy K. M., Rao K. N., Lingaiah N., and Saiprasad P. S., Structure and reactivity of zirconium oxide-supported ammonium salt of 12-molybdophosphoric acid catalysts. *J. Appl. Catal. A: Gen.*, **300**, 139-146 (2006).
- Salama R. S., El-Hakam S. A., Samra S. E., El-Dafrawy Sh. M., Ahmed A. I., Cu-BDC as a Novel and Efficient Catalyst for the Synthesis of 3,4-Dihydropyrimidin-2(1H)-ones and Aryl-14H-dibenzo [a, j] Xanthenes under Conventional Heating. *Intern. J. of Nano and Mater. Scien.*, **7**(1), 31-42 (2018).
- Devassy B. M., Lefebvre F., Bohringes W., Fletcher J., and Halligudi S. B., Synthesis of linear alkyl benzenes over zirconia-supported 12-molybdophosphoric acid catalysts. *J. Mol. Catal. A: Chem.*, **236**, 162-167 (2005).
- El-Hakam S. A., El-Khouly A. A., Khder A. S., Effect of thermal treatment on various characteristics of nickel/aluminum phosphate catalysts. *J. Appl. Catal. A: Gen.*, **185**, 247-257 (1999).
- El-Hakam S. A., Hassan Sh. M., Ahmed A. I. and Farag H. M., Structure, Texture and Catalytic Properties of Pd/SiO_2 . *Catalysts*, **13**, 423-431(1996).
- El-Dafrawy Sh. M., Youssef H. M., Toamah W. O. *Egypt. J. Chem.* **62**, No. 12 (2019)

- and El-Defrawy M. M., Synthesis of Nano-CaO Particles and Its Application for the Removal of Copper (II), Lead (II), Cadmium (II) and Iron (III) from Aqueous Solutions, *Egypt. J. Chem.*, **58**(6), 579-589 (2015).
16. Sethna S. and Phadke S. M., *The Pechmann Reaction J. Org. React.*, **7**, 1-7(1953).
17. Shockravib A. and Valizadeha H., An efficient procedure for the synthesis of coumarin derivatives using $TiCl_4$ as catalyst under solvent-free conditions *J. Tetrahed. Lett.*, **46**, 3501-3503(2005).
18. El-Dafrawy Sh. M., Synthesis, Characterization and Catalytic Activity Cobalt Doped Nano Sulphated Zirconia Catalyst: A Study of Cumarin Pechman Synthesis. *Inter. J. of Scienc. and Resear.*, **4**, 1538-1542 (2015).
19. Salam R. S., El-Hakam S. A., Samra S. E., El-Dafrawy Sh. M., Ahmed A. I., Adsorption, Equilibrium and Kinetic Studies on the Removal of Methyl Orange Dye from Aqueous Solution by Using of Copper Metal Organic Framework (Cu-BDC), *Intern. J. of Modern Chem.*, **10** (2), 195-207 (2018).
20. Reddy B. M., Reddy G. K., Rao K. N., Katta L., Influence of alumina and titania on the structure and catalytic properties of sulfated zirconia: Beckmann rearrangement. *J. Molec. Catal. A: Chem.*, **306**, 62-68 (2009).
21. Navio J. A., Hidalgo M. C., Colon G., Botta S. G., and Litter M. I., Preparation and Physicochemical Properties of ZrO_2 and Fe/ZrO_2 Prepared by a Sol-Gel Technique. *J. Langmuir*, **17**, 202-210 (2001).
22. Sirinivasan R., and Davis B. H., Glow Phenomenon and Crystallization: Evidence That They Are Different Events for Hafnium-Zirconium Mixed Oxides. *J. Coll. Interface Scin.*, **156**, 400-405 (1993).
23. Pae Y. I., Lee S. H., Sohn J. R., Correlation between acidic properties of nickel sulfate supported on TiO_2-ZrO_2 and catalytic activity for ethylene dimerization. *J. Catal. Lett.*, **99**, 241-248 (2005).
24. Landau J. V., Vradman L., Wang X. and Titelman L., High loading TiO_2 and ZrO_2 nanocrystals ensembles inside the mesopores of SBA-15: preparation, texture and stability. *J. Micro. Meso. Mater.* **78**, 117-129 (2005).
25. Zou H. and Lin Y. S., Structural and surface chemical properties of sol-gel derived TiO_2-ZrO_2 oxides. *J. Appl. Catal. A: Gen.*, **265**, 35-42 (2004).
- Egypt. J. Chem.* **62**, No. 12 (2019)
26. Sohn J. R., Lee S. H., Effect of TiO_2-ZrO_2 composition on catalytic activity of supported $NiSO_4$ for ethylene dimerization. *J. Appl. Catal. A: Gen.* **321**, 27-34 (2007).
27. Afanasiev P., Mixed TiO_2-ZrO_2 support for hydrotreating, obtained by co-precipitation from Zr basic carbonate and Ti oxosulfate. *J. Catal. Comm.*, **9**, 734-739 (2008).
28. Lonyi F., and Valyon J., Thermally effected structural and surface transformations of sulfated TiO_2 , ZrO_2 and TiO_2-ZrO_2 catalysts. *J. Therm. Anal.*, **46**, 211-218 (1996)
29. Lu Q., Zhang Y., Tang Z., Li W. Z., Zhu X. F., Catalytic upgrading of biomass fast pyrolysis vapors with titania and zirconia/titania based catalysts. *J. Fuel*, **89**, 2096-2103 (2010).
30. Lai S. Y., Pan W., Ng C. F., Catalytic hydrolysis of dichlorodifluoromethane (CFC-12) on unpromoted and sulfate promoted TiO_2-ZrO_2 mixed oxide catalysts. *J. Appl. Catal. B: Envir.*, **24**, 207-217 (2000).
31. Rodrigues C. M., Ferreira O. P., Alves O. L., Nanostructures of sodium titanate/zirconium oxide. *J. Nanopart. Reser.*, **12**, 2355-2361(2010).
32. Kim J. Y., Kim C. S., Chang H. K., Kim T., Effects of ZrO_2 addition on phase stability and photocatalytic activity of ZrO_2/TiO_2 nanoparticles, *J. Advan. Powd. Techn.*, **21**, 141-144 (2010).
33. Mishra T., Anion supported TiO_2-ZrO_2 nanomaterial synthesized by reverse microemulsion technique as an efficient catalyst for solvent free nitration of halobenzene. *J. Catal. Comm.*, **9**, 21-26 (2008).
34. Ahmed A. I., El-Hakam S. A., S Samra. E., EL-Khouly A. A., Khder A. S., Structural characterization of sulfated zirconia and their catalytic activity in dehydration of ethanol. *J. Coll. Surf. A: Phys. chem. Eng. Aspects*, **317**, 62-70 (2008).
35. Li Y., Zhang X. D., Sun L., Zhang J., Xu H. P., Fatty acid methyl ester synthesis catalyzed by solid superacid catalyst $SO_4^{2-}/ZrO_2-TiO_2/La^{3+}$, *J. Appl. Energ.*, **87**, 156-159 (2010).
36. Wan Y., Ma J., Zhou W., Zhu Y., Song X., Lia H., Preparation of titania-zirconia composite aerogel material by sol-gel combined with supercritical fluid drying. *J. Appl. Catal. A: Gen.*, **277**, 55-59 (2004).

37. Velmurugan R., Krishnakumar B., Swaminathan M., Synthesis of Pd co-doped nano-TiO₂-SO₄²⁻ and its synergetic effect on the solar photodegradation of Reactive Red 120 dye, *J. Mater. Sci. in Semicond. Proc.*, **25**, 163-172 (2014).
38. Khan I., Khan S., Nongjai R., Ahmed H., Khan W., Structural and optical properties of gel-combustion synthesized Zr doped ZnO nanoparticles. *J. Optical Mater.*, **35**, 1189-1193 (2013).
39. Li D., Ohashi N., Hishita S., Kolodiazny T., and Haneda H.; Origin of visible-light-driven photocatalysis: A comparative study on N/F-doped and N-F-codoped TiO₂ powders by means of experimental characterizations and theoretical calculations. *J. Sol. State Chem.*; **178**, 3293-3302 (2005).
40. Li S-X., Cai S-J., Zheng F-Y., Self assembled TiO₂ with 5-sulfosalicylic acid for improvement its surface properties and photodegradation activity of dye, *J. Dyes and Pigm.*, **95**, 188-193 (2012).
41. Fathinia M., Khataee A. R., Zarei M., Aber S., Comparative photocatalytic degradation of two dyes on immobilized TiO₂ nanoparticles: Effect of dye molecular structure and response surface approach. *J. Mol. Catal. A: Chem.*, **333**, 73-84 (2010).
42. El-Dafrawy Sh. M., Structural and Photocatalytic of MCM Doped ZnO Nanoparticles, and It's Application in Removal of Iron, Cadmium and Lead Ions from Water. *Journal of Catal. and Catal. Resear.*, **1**, 1-9 (2015).
43. El-Hakam S. A., Samra S. E., El-Dafrawy Sh M., Ibrahim A. A., Salama R. S., Ahmed A. I., Synthesis of sulfamic acid supported on Cr-MIL-101 as a heterogeneous acid catalyst and efficient adsorbent for methyl orange dye. *J. RSC Adv.*, **8**, 20517-20533 (2018).
44. Wang J., Xie Y., Zhang Z., Li J., Chen X., Zhang L., Xu R., Zhang X., Photocatalytic degradation of organic dyes with Er³⁺:YAlO₃/ZnO composite under solar light. *J. Sol. Mater.*, **93**, 355-361 (2009).

محفز تيتانيوم-زركونيا بحجم النانو تم تعديله بواسطة كبريتات كمحفز فعال

شادي محمد محمد الدفراوي

قسم الكيمياء - كلية العلوم - جامعة المنصورة - المنصورة - مصر.

تم تحضير سلسلة من محفز Titanium Zirconia باستخدام تقنية sol-gel المعدل بالكبريتات. تم تحميل جميع العينات في عدة درجات حرارة 500 و 600 و 750 درجة مئوية لمدة 3 ساعات. واستخدمت أساليب التحقيق من الخصائص الهيكلية مثل؛ التحليل الحراري، حيود الأشعة السينية (XRD)، المجهر الإلكتروني النافذ (TEM)، ومسح المجهر الإلكتروني (SEM) بالإضافة إلى ذلك، تم تقييم الميزات السطحية من خلال الامتزاز في درجة حرارة منخفضة من N₂ في -196 درجة مئوية. تم تحديد قياس الحموضة السطحية مع معايرة ن- بوتيل أمين في الأسيتونيتريل. تم استخدام تفاعل بيكمان لإنتاج الكومارين في اختبار النشاط الحفاز للعوامل الحفازة المشيدة. تم قياس الكفاءة الضوئية لصبغة الميثيلين الزرقاء للحفازات المحضرة.